Spectroscopy of ^{90}Nb at high spin

A. Chakraborty,* Krishichayan, S. S. Ghugre, R. Goswami, S. Mukhopadhyay, N. S. Pattabiraman, S. Ray, and A. K. Sinha
UGC-DAE Consortium for Scientific Research, Kolkata Center, Sector III/LB-8, Bidhan Nagar, Kolkata 700098, India

S. Sarkar
Department of Physics, The University of Burdwan, Burdwan 713104, India

P. V. Madhusudhana Rao and U. Garg
Department of Physics, University of Notre Dame, Notre Dame, Indiana 46556, USA

S. K. Basu
Variable Energy Cyclotron Center, Sector-I/AF, Bidhan Nagar, Kolkata 700064, India

M. B. Chaterjee and M. Saha Sarkar
Saha Institute of Nuclear Physics, Sector-I/AF, Bidhan Nagar, Kolkata 700064, India

L. Chaturvedi, A. Dhal, and R. K. Sinha
Department of Physics, Banaras Hindu University, Varanasi 221005, India

I. M. Govil
Department of Physics, Panjab University, Chandigarh 160014, India

R. K. Bhowmik, A. Jhingan, N. Madhavan, S. Muralithar, S. Nath, R. P. Singh, and P. Sugathan
Nuclear Science Center, Aruna Asaf Ali Marg, New Delhi 110067, India
(Received 3 November 2004; revised manuscript received 1 August 2005; published 16 November 2005)

Excited states of ^{90}Nb were investigated via prompt and delayed γ decays and the recoil-isomer tagging technique. The level scheme of ^{90}Nb has been extended up to $J = 19\hbar$ and $E_x = 8.4$ MeV. Half-lives of the 11^- and $17/2^-$ isomeric levels in ^{90,91}Nb were measured to be 0.47 ± 0.01 and 3.3 ± 0.4 μs, respectively. The results are compared with the predictions of large-basis shell model calculations. The effects of truncation of the valence model space on the calculated results are discussed.

DOI: 10.1103/PhysRevC.72.054309 PACS number(s): 27.60.+j, 23.20.Lv, 21.10.Tg, 21.60.Cs

I. INTRODUCTION

The study of odd-odd nuclei offers a scope for investigating the underlying proton-neutron residual interactions. Such nuclei exhibit highly complex level structures because of a large number of possible couplings of the odd proton and neutron to the even-even core. The odd-odd nucleus ^{90}Nb, with 41 protons and 49 neutrons, is one such interesting candidate in the $A \sim 90$ region, with both the proton-particle and the neutron-hole occupying the $1g_{9/2}$ orbital. From the shell model point of view, nuclei in this mass region have generally been described in the valence spaces above the $^{88}_{38}Sr_{50}$ and $^{76}_{38}Sr_{38}$ cores for many years. The calculations, involving the $(2p_{1/2}, 1g_{9/2})$-valence space and assuming $Z = N = 38$ subshell closure in $^{76}_{38}Sr_{38}$, have been found to be quite successful in describing the low-lying levels for nuclei in this mass region, particularly for ^{90}Nb up to $J \sim 12\hbar$ [1,2].

The low-lying level structure of ^{90}Nb was investigated earlier by several workers using direct reactions [3–5] and γ-spectroscopic techniques [6,7]. The study by Fields *et al.* [7] provided information on the level structure of ^{90}Nb up to an excitation energy of $E_x \sim 3$ MeV and spin $J \sim 12\hbar$. The said authors also reported an 11^- isomeric level with a half-life of 0.44 ± 0.02 μs, using delayed coincidence measurement. Incidentally, the same isomer was studied earlier by Häusser *et al.* [8].

According to the latest compilations in Nuclear Data Sheets [9], there is hardly any information on the level structure of ^{90}Nb above the 11^- isomeric level. It is, therefore, of interest to investigate the level structure of ^{90}Nb to a higher spin and excitation energy, where one expects to observe states arising out of the excitation of nucleons across both the $Z = 38$ subshell and $N = 50$ shell closure. Similar states have indeed been observed recently by our group [10,11] in ^{91,92}Mo and by Hausmann *et al.* [12] in ^{93}Tc nuclei.

Fields *et al.* [7] has also suggested an additional contribution in the half-life of the 813-keV ($9^+ \rightarrow 8^+$) transition, from the decay of the 11^- isomeric level. However, the authors could not determine its half-life with certainty because of contamination from another 813-keV γ ray in ^{89}Mo, produced in their reaction. The additional motivation of this work has

*Present address: Department of Physics, Krishnath College, Berhampore 742101, India.

been to explore this unidentified isomer and to search for new isomers in the neighboring nuclei.

We have measured the half-lives of the 11^- and $17/2^-$ isomeric levels in ^{90,91}Nb, respectively, using the recoil-isomer tagging technique. This technique has the advantage of studying the decay of the isomeric levels from specific nuclei in a low-background environment using the selectivity of a recoil-mass analyzer and thereby it eliminates the contributions, if any, from the neighboring nuclei, which was not possible in the work of Fields *et al*. [7]. Besides, it allows us to correlate the feeding and decay pattern of the tagged isomers. In this work, we used the prompt-delayed coincidences to identify the transitions across the 11^- isomeric level in ^{90}Nb. Prompt $\gamma\gamma$ coincidences were, then, used to extend the level scheme above the isomeric level.

More than 15 new transitions have been identified and placed in the level scheme, leading to a considerable extension of the level structure of ^{90}Nb up to $E_x \sim 8$ MeV and $J \sim 19\hbar$. The observed level structure is irregular, similar to what is expected for a near-spherical nucleus, and indicates the persistence of single-particle behavior up to the highest observed spin and excitation energy. This makes the spherical shell model an appropriate means to interpret the observed level structure. As mentioned earlier, theoretical studies on the structure of ^{90}Nb using the shell model have been performed by several authors [1,2]. In this work, shell model calculations have been performed using different Hamiltonians in the subspaces of the model space $\pi(1f_{5/2}, 2p_{3/2}, 2p_{1/2}, 1g_{9/2})$ and $\nu(2p_{1/2}, 1g_{9/2}, 1g_{7/2}, 2d_{3/2}, 2d_{5/2}, 3s_{1/2})$. The theoretical predictions have been compared with the experimental observables such as level spectra, electromagnetic transition probabilities, and branching ratios. A reasonable agreement between the experimental and calculated results has been found.

II. EXPERIMENTAL DETAILS AND DATA ANALYSIS

The excited states of ^{90}Nb were populated using the ^{63}Cu(^{31}P, $3p1n$) reaction in two separate experiments at beam energies of $\sim$120 and 125 MeV, respectively. In one of the experiments, we used a $\sim$1.2 mg/cm^2 thick and enriched ^{63}Cu target on a gold backing of thickness 10 mg/cm^2. The 125-MeV ^{31}P beam was provided by the 14 UD Pelletron accelerator at the Tata Institute of Fundamental Research (TIFR), Mumbai. The deexciting γ rays were detected using an early implementation of the Indian National Gamma Array (INGA), consisting of eight Compton-suppressed Clover detectors and a 14-element NaI(Tl) multiplicity filter [10]. The detectors were placed in the median plane at 60°, 90°, 120°, 150°, 210°, 250°, 285°, and 325°, with respect to the beam direction. The master trigger was generated by a coincidence condition in which three or more Clover detectors had fired, along with a $K \geqslant 2$ multiplicity condition for the NaI(Tl) multiplicity filter. In all, about 205 million $\gamma\gamma\gamma$ coincidence events were accumulated in list mode. In order to confirm the coincidences between the prompt transitions above the 11^- isomeric level and the known transitions below this isomer, a second experiment was performed at the Nuclear Science Centre (NSC), New Delhi, using the 15 UD Pelletron facility. The ^{63}Cu(^{31}P, $3p1n$) reaction at a beam energy of 120 MeV was employed. The target consisted of a self-supporting foil of ^{63}Cu with thickness $\sim$760 μg/cm^2. The experimental arrangement comprised the INGA facility, coupled to the Heavy Ion Reaction Analyzer (HIRA) [13]. The recoil-isomer tagging technique was employed, wherein the γ-ray measurements were made both at the target position and at the focal plane of the HIRA. The prompt γ transitions feeding the isomeric levels were detected in the Clover array at the target position. A standard 23% HPGe detector was placed close to the end flange of the focal plane of the HIRA to detect the delayed γ rays originating from the decay of the isomeric levels in the nuclei, which were selectively transported to the focal plane of the HIRA. The details of the experimental setup are given in a previous work [14]. The data were recorded when either (a) a $\gamma\gamma$ coincidence was detected by the Clover array or (b) a γ ray was detected by the array in coincidence with a selected recoiling nucleus at the HIRA focal plane. The arrival of the nuclei in an isomeric state at the focal plane started a time-to-amplitude converter (TAC) which was then stopped by the electronically delayed HPGe signal, indicating the detection of γ rays following the decay of the isomer. This delayed time information t from TAC along with the energy information $E_{d\gamma}$ from the HPGe detector were recorded in list mode along with the prompt $\gamma\gamma$ coincidences between the Clover detectors. The zero time, corresponding to the arrival of the isomeric nucleus at the focal plane of the HIRA, was obtained from the anode signal of a multiwire proportional counter (MWPC). Around 600 million prompt $\gamma\gamma$ coincident events and approximately 2 million prompt-delayed $\gamma\gamma$ coincident events were recorded.

As no in-beam data were recorded in singles mode, the HIRA transmission efficiency for ^{90}Nb could not be experimentally determined. However, simulations [15] have shown that for the HIRA acceptance set with a 5 msr solid angle, the efficiency for $A = 90$ nuclei reaching the focal plane is $\sim$2.2%. This value increases to about 3.0% for the 10 msr setting. These values have a maximum uncertainty of $\pm$20%. The data have mostly been accumulated using the 5 msr setting.

As mentioned earlier, the recoil-isomer tagging technique has a dual advantage. Besides establishing the half-lives of the isomeric levels, it also allows us to correlate between the prompt transitions feeding the isomeric level and the delayed transitions originating from the decay of the isomer. The level scheme for the nuclei of interest could then be developed across the isomeric level from these prompt-delayed coincidences. Indeed, because of the nonavailability of data on the level structure of ^{90}Nb above the 11^- isomeric level prior to this work, the prompt-delayed coincidences were essential for establishing the level scheme across the isomeric level.

The data analysis was performed using the Linux-based γ^N analysis software packages IUCSORT [16,17] and RADWARE [18]. Besides the conventional prompt γ^N ($N = 2, 3$) histograms, prompt-delayed and $E_{d\gamma}$-t matrices were also constructed. The half-lives of the isomeric levels were obtained from the $E_{d\gamma}$-t matrix. One axis of this matrix corresponds

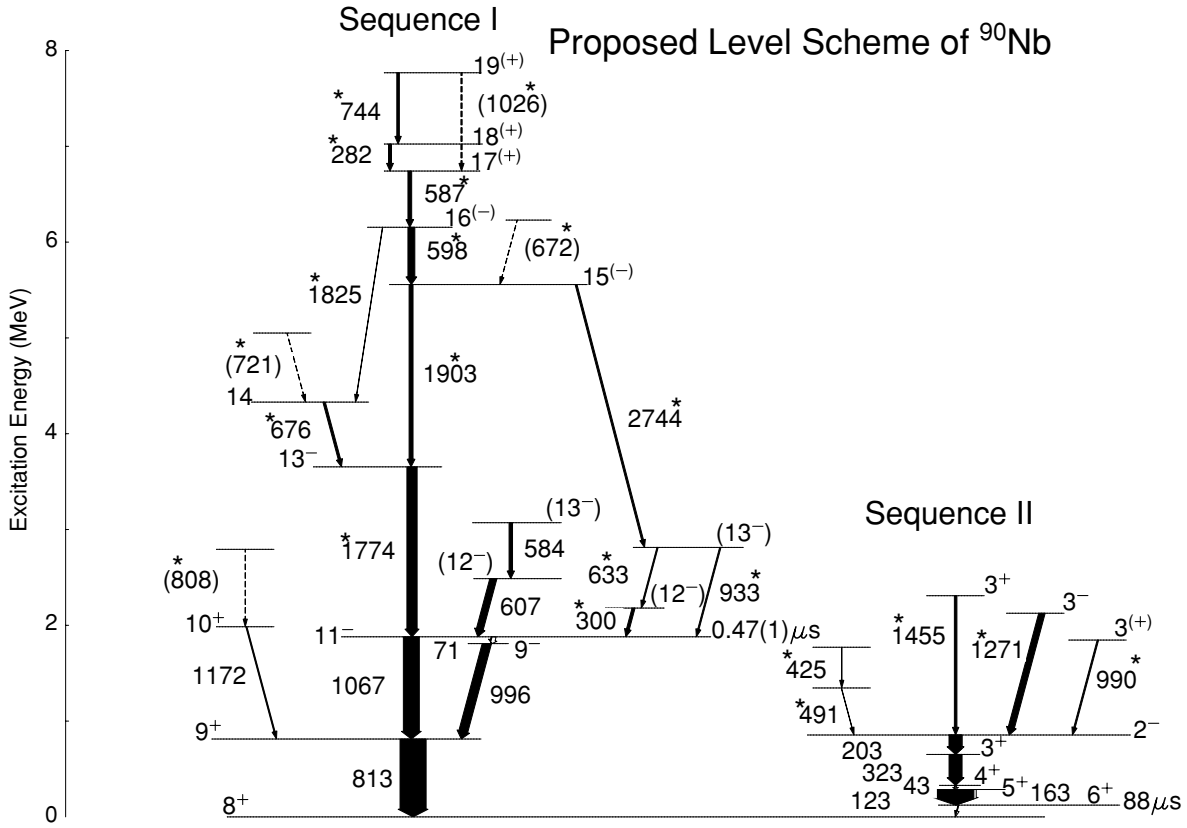

FIG. 1. Proposed level scheme for ^{90}Nb. Newly observed transitions are marked with an asterisk. Widths of arrows connecting the levels are proportional to the relative γ-ray intensities.

to the time difference between the detection of a recoil by the MWPC and that of a decay γ ray in the HPGe detector; and the other axis, to the corresponding γ-ray energy. The delayed γ-ray spectra were then projected with successive time slices on the recoil-γ TAC, having 0.5 and 1.0 μs widths, respectively.

Seventeen new γ transitions belonging to ^{90}Nb were identified and placed in the decay scheme (Fig. 1). A representative prompt-delayed coincidence spectrum, from the self-supporting target experiment (performed at NSC), with gates on the transitions originating from the decay of the known 11^- isomeric level in ^{90}Nb, is shown in Fig. 2(a); Fig. 2(b) illustrates the $\gamma\gamma\gamma$ coincidence (prompt) spectrum from the backed target experiment (performed at TIFR). Further, Fig. 2(c) depicts the coincidences between the transitions depopulating the high spin states of Sequence I with the newly reported 1774-keV transition which feeds the 11^- isomeric level. Figure 2(d) shows the gated spectrum of the newly observed 2744-keV γ transition. The coincidences between the members of the low-lying Sequence II is indicated in Fig. 2(e). The available data did not indicate any linking transitions between Sequences I and II.

The angle-dependent E_γ-E_γ matrices, with the data from the backed-target experiment, were used to obtain the intensity ratios for the γ transitions; these, in turn, were used to assign qualitatively the spin of the proposed levels. These assignments were based on the assumptions of stretched transitions for the gates, and all calculations were performed after incorporating the necessary efficiency corrections. The multipolarity assignments were carried out using the procedure described in Ref. [19]. A $\gamma\gamma$ matrix was constructed with one axis corresponding to the data recorded in the 150°, 210°, and 325° detectors; the other axis contained the coincidence data from the 90°, 250°, and 285° detectors. We then define $R_{\rm int}$ as

$$R_{\rm int} = \frac{I_{\gamma_1} \text{ at } 90^\circ, 250^\circ, \text{ and } 285^\circ;\ \text{gatedwith } \gamma_2 \text{ at } 150^\circ, 210^\circ, \text{ and } 325^\circ}{I_{\gamma_1} \text{ at } 150^\circ, 210^\circ, \text{ and } 325^\circ;\ \text{gatedwith } \gamma_2 \text{ at } 90^\circ, 250^\circ, \text{ and } 285^\circ}.$$

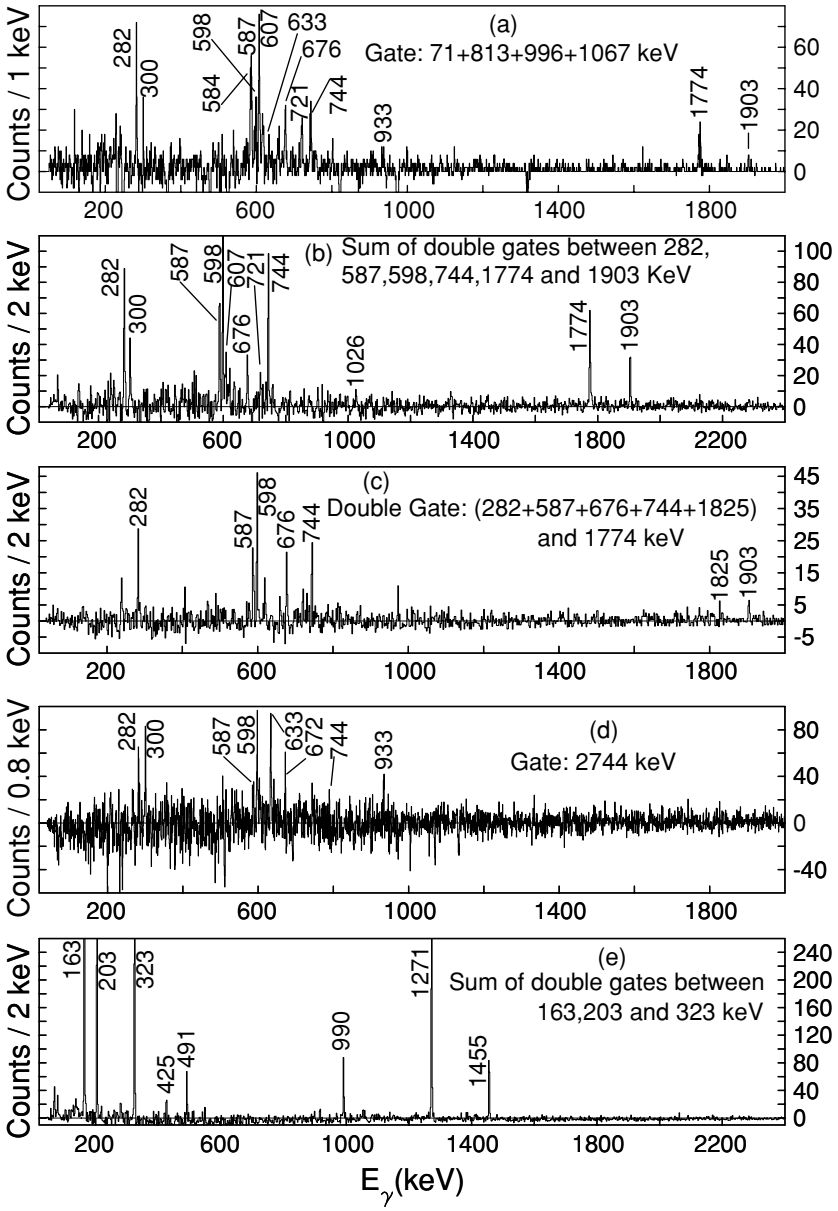

FIG. 2. (a) Prompt-delay coincidence spectrum (from the NSC experiment). (b) Prompt correlation spectrum of the observed transitions above the 11^- isomeric state (from the TIFR experiment) of Sequence I. (c) $\gamma\gamma\gamma$ coincidence spectrum between the 1774-keV and some of the other prompt transitions of Sequence I. (d) $\gamma\gamma$ coincidence spectrum gated by the newly observed 2744-keV transition of Sequence I. (e) $\gamma\gamma\gamma$ coincidence spectrum for Sequence II. Peaks labeled by their energy values are assigned to ^{90}Nb.

Assuming the commonly encountered situation of stretched transitions, the value of $R_{\rm int}$ for those γ rays having the same multipolarity as the gated γ ray would be $\sim$1, while the value differs by a factor of $\sim$2 if the multipolarities of the γ rays are different. The resultant values of $R_{\rm int}$ for some of the observed transitions are illustrated in Fig. 3(a). The polarization sensitivity of Clover detectors was used to assign qualitatively the parities for some of the observed levels. As described in Refs. [20,21], the asymmetry parameter $\Delta_{\rm IPDCO}$ was obtained using the relation

$$\Delta_{\rm IPDCO} = \frac{[a(E_\gamma)N_\perp] - N_\parallel}{[a(E_\gamma)N_\perp] + N_\parallel},$$

where the γ-ray energy-dependent function $a(E_\gamma)$ corresponds to the geometrical asymmetry of the detector array, and $N_\perp$ and $N_\parallel$ correspond to the number of perpendicular and parallel scatters, respectively, for a given γ ray. An electric transition would result in a positive value for the asymmetry parameter; whereas a negative value corresponds to a magnetic transition. A near-zero value for the asymmetry parameter is indicative of an admixture. Fig. 3(b) illustrates the value of the asymmetry parameter for some of the observed transitions in ^{90}Nb. For comparison, we have included a few known transitions from ^{90}Mo [22], which was one of the dominant fusion evaporation residues produced in the present reaction.

III. EXPERIMENTAL RESULTS

A. The level scheme of ^{90}Nb

As seen from Fig. 1, the level scheme of ^{90}Nb has been extended up to $E_x \sim 8$ MeV and $J = 19\hbar$. The newly observed transitions have been marked with an asterisk. The level and transition energies, γ-ray intensities, DCO and IPDCO ratios, and deduced spin-parity assignments are summarized in Table I. The intensities of the observed transitions

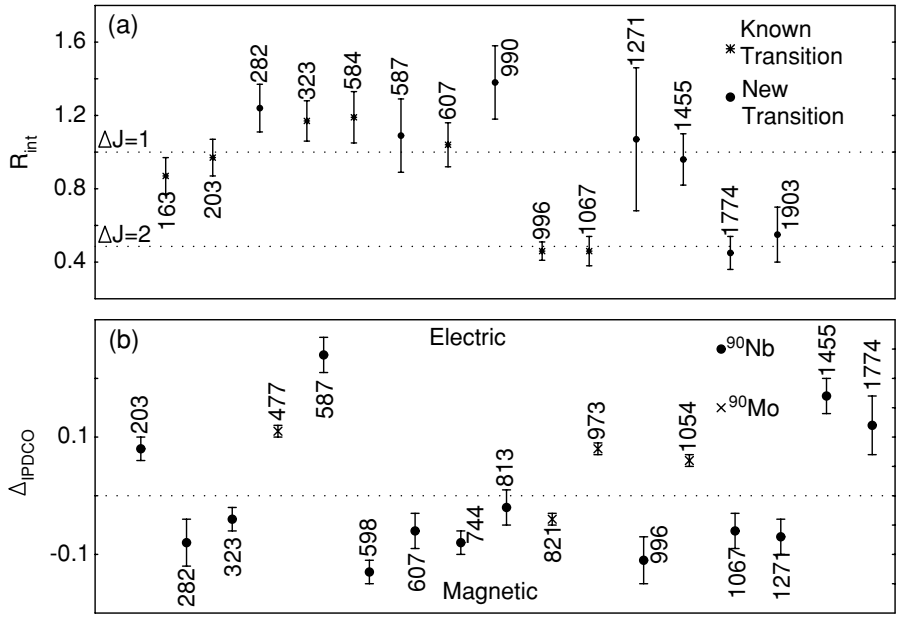

FIG. 3. (a) $R_{\rm int}$ values for some of the transitions belonging to ^{90}Nb. Dotted lines correspond to values obtained for known dipole and quadrupole transitions and have been drawn to guide the eye. Gating transition is of a dipole nature for both the $\Delta J = 1$ and $\Delta J = 2$ transitions. Quoted error includes the error due to background subtraction, fitting, and efficiency correction. (b) Experimental γ-ray asymmetry parameter obtained from polarization measurement. Quoted error encompasses error due to background subtraction and fitting. Dotted line through the zero value of the asymmetry parameter has been drawn to guide the eye.

(lying above the 11^- isomeric level) belonging to Sequence I have been obtained from the added spectra, corresponding to the 813-keV ($9^+ \rightarrow 8^+$), 1067-keV($11^- \rightarrow 9^+$), 996-keV ($9^- \rightarrow 9^+$), and 71-keV ($11^- \rightarrow 9^-$) gated transitions, and were normalized with respect to the earlier reported intensity for the 607-keV ($(12_2^-) \rightarrow 11^-$) transition [7].

The intensities of the low-lying transitions belonging to the same sequence, viz., 71-, 996-, 1067-, and 1172-keV, have been obtained from the 813-keV gated spectrum and were normalized with the known intensity of 607 keV. The intensity of the 813-keV transition has been obtained by summing the normalized intensities of the 996-, 1067-, and 1172-keV transitions. The intensity of the 203-keV ($2^- \rightarrow 3^+$) transition, belonging to Sequence II, has been obtained from the 163-keV($5^+ \rightarrow 6^+$) gated spectrum and normalized to the known intensity of the 323-keV ($3^+ \rightarrow 4^+$) transition [7]. The sum coincident spectra of the 163- and 323-keV transitions, together with normalization to the intensity of the 203-keV transition, have been used to obtain the intensity of the newly observed 425-, 491-, 990-, 1271-, and 1455-keV transitions. However, it was observed in the spectra, with necessary efficiency corrections, gated by the 1903- and 203-keV transitions, that the number of counts in the photopeaks corresponding to the 1774- and 323-keV transitions (which lie immediately below the respective gating transitions) is nearly identical. This is indicative of similar feeding patterns for these two sequences. The intensities of the 1774- and 203-keV photopeaks were measured from the efficiency-corrected projection spectrum. This is based on the assumption that these two transitions are relatively contaminant free. Comparing these counts with the relative efficiencies obtained with the aforementioned procedure, it is found that the normalization requires an increase by a factor of $\sim$3.4 for Sequence II in order to have its intensity comparable with that of Sequence I. This has been incorporated in determining the final intensities reported herein.

We have observed almost all transitions previously reported by Fields *et al.* [7] as belonging to ^{90}Nb. However, they had placed two single γ rays, of energies 238-keV ($5^- \rightarrow 4^-$) and 171-keV ($7^+ \rightarrow 8^+$), that have not been included in the present level scheme because of lack of coincidence information on these γ transitions. Also, the 43-keV transition could not be detected in these experiments and the 123-keV γ ray (the lowest transition in Sequence II) was not seen within the prompt coincidence time window. The decay of the reported isomeric level ($T_{1/2} = 88\ \mu$s) [9] at $J^\pi = 6^+$ could not be investigated in our measurement, which was limited to half-lives of a few microseconds. It is observed that the nonyrast 13^- state has a higher feeding than that of the corresponding yrast state. Such an observation is reported as well by Rzaca-Urban *et al.* [23] for ^{144}Gd. This feature is indeed intriguing and warrants further investigation, both on theoretical and experimental fronts, but is beyond the scope of the present study. It might be attributable to the nature of the wave functions of these states. The shell model calculations, as discussed in the subsequent section, indicate that the $\pi(1f_{5/2}^5, 2p_{3/2}^4, 1g_{9/2}^4) \otimes \nu(2p_{1/2}^2, 1g_{9/2}^9)$ configuration, where the notation $1f_{5/2}^n$ denotes the n number of particles in the orbital $1f_{5/2}$, dominates the $15^{(-)}$ as well as the 13_3^- state. This may result in a preferential feeding to this nonyrast state.

The present measurements confirm the dipole nature of the 813-keV transition and the quadrupole nature of both the 1067- and 71-keV transitions (belonging to Sequence I), which are in agreement with the assignments of Fields *et al.* [7]. Our measurements indicate that the 996-keV transition involves $\Delta J = 0, 2$. The polarization measurement is indicative of a magnetic nature for this transition. Fields *et al.* [7] had assigned this transition as a $\Delta J = 0$, $E1$ transition. We are, however, in favor of an $M2$ assignment for this transition.

Theoretical angular correlation calculations were carried out using the ANGCOR code (unpublished) for a few low-lying

TABLE I. γ transition energies (E_γ) in keV, excitation energies (E_x) in keV, relative γ-ray intensities (I_γ), DCO ratios ($R_{\rm int}$), IPDCO ratios ($\Delta_{\rm IPDCO}$), multipolarities, and initial and final spins for the transitions belonging to ^{90}Nb.

E_γ	E_x	I_γ[a]	$R_{\rm int}$	Gate	$\Delta_{\rm IPDCO}$	Multipolarity	$J_i^\pi \rightarrow J_f^\pi$
42.5[b,c]	328	2(1)				$M1$	$4^+ \rightarrow 5^+$
70.8	1880	1.7(3)	1.35(23)	996[d]		$E2$	$11^- \rightarrow 9^-$
122.6[b,c]	123	51(3)				$E2$	$6^+ \rightarrow 8^+$
163.0	286	67.9(34)	0.87(10)	323[e,f]		$M1$	$5^+ \rightarrow 6^+$
203.3	855	22.3(25)	0.97(10)	163[e]	0.08(2)	$E1$	$2^- \rightarrow 3_1^+$
281.9	7024	5.1(9)	1.24(13)	598[e]	−0.08(4)	$M1$	$18^{(+)} \rightarrow 17^{(+)}$
300.4	2181	5.0(9)				$M1$	$(12_1^-) \rightarrow 11^-$
323.3	651	22.4(14)	1.17(11)	163[e,f]	−0.04(2)	$M1$	$3_1^+ \rightarrow 4^+$
425.0	1770	w[g]					
490.6	1345	w[g]					$\rightarrow 2^-$
584.3	3072	6.0(11)	1.19(14)	607[e]		$M1$	$(13_2^-) \rightarrow (12_2^-)$
586.8	6742	6.5(12)	1.09(20)	598[e]	0.24(3)	$E1$	$17^{(+)} \rightarrow 16^{(-)}$
597.7	6155	11.9(21)	2.08(20)	1774[d]	−0.13(2)	$M1$	$16^{(-)} \rightarrow 15^{(-)}$
607.0	2487	12(2)[c]	1.04(12)	813[e,h]	−0.06(3)	$M1$	$(12_2^-) \rightarrow 11^-$
633.2	2814	2.0(4)				$M1$	$(13_1^-) \rightarrow (12_1^-)$
672.1	6230	w[g]					$\rightarrow 15^{(-)}$
676.4	4331	4.1(7)	2.00(21)	1774[d]		Dipole	$14 \rightarrow 13_3^-$
720.6	5051	w[g]					$\rightarrow 14$
744.0	7768	4.4(8)	1.96(53)	1774[d]	−0.08(2)	$M1$	$19^{(+)} \rightarrow 18^{(+)}$
807.7	2793	w[g]					$\rightarrow 10^+$
813.4	813	45.3(88)	2.02(24)	1067[d,f]	−0.02(3)	$M1$	$9^+ \rightarrow 8^+$
933.3	2814	2.2(4)				$E2$	$(13_1^-) \rightarrow 11^-$
990.4	1845	2.3(2)	1.38(20)	203[e]		$E1$	$3_2^{(+)} \rightarrow 2^-$
996.2	1810	15.7(31)	0.46(5)	813[e]	−0.11(4)	$(M2)$	$9^- \rightarrow 9^+$
1025.7	7768	2.1(4)	1.17(60)	1774[d]		$E2$	$19^{(+)} \rightarrow 17^{(+)}$
1066.8	1880	27.7(54)	0.46(8)	813[e,f]	−0.06(3)	$M2$	$11^- \rightarrow 9^+$
1172.1	1986	1.9(4)				$M1$[i]	$10^+ \rightarrow 9^+$
1271.3	2126	10.9(8)	1.07(39)	203[e]	−0.07(3)	$M1$	$3^- \rightarrow 2^-$
1454.7	2309	4.2(3)	0.96(14)	323[e]	0.17(3)	$E1$	$3_3^+ \rightarrow 2^-$
1773.9	3654	17.7(31)	0.45(9)	587[e]	0.12(5)	$E2$	$13_3^- \rightarrow 11^-$
1824.9	6155	w[g]				Quadrupole	$16^{(-)} \rightarrow 14$
1903.4	5558	6.8(12)	0.55(15)	598[e]		$E2$	$15^{(-)} \rightarrow 13_3^-$
2744.2	5558	3.2(6)				$E2$	$15^{(-)} \rightarrow (13_1^-)$

[a]The quoted errors on intensities include errors due to background subtraction, fitting, and efficiency correction.
[b]Not observed in the present expt.
[c]Taken from the Ref. [7].
[d]Gating transition is of quadrupole nature.
[e]Gating transition is of dipole nature.
[f]Spin and parity already known from Ref. [7].
[g]Corresponds to weak transitions whose intensity could not be computed.
[h]Gating transition lies below the isomeric level (see text).
[i]Taken from Ref. [7] and could not be computed in the present investigation because of poor statistics.

transitions. The value of σ used in this calculation has been taken from Ref. [24]. Here, σ refers to the Gaussian width of the m-substate distribution of the initial level. Since the mixing ratios for the transitions are not available, the theoretical $R_{\rm int}$ values for the same could not be calculated unambiguously. It is observed that the theoretical $R_{\rm int}$ value for 996-keV transition, assuming $E1$ multipolarity (with 10% $M2$ admixture) is in good agreement with the deduced experimental value. However, the calculation indicates a significant difference between the experimental and theoretical $R_{\rm int}$ values for a pure $M2$ nature of the 996-keV transition. If one assumes an $M2$ nature for this transition, the lifetime would be typically about 1 ns, from Weisskopf single-particle estimates [25], which corresponds to the prompt coincidence timing interval. A similar assignment of a 1098-keV $M2$ transition has been reported in ^{92}Mo by Pattabiraman *et al.* [11]. Based on the above, an $M2$ multipolarity has been tentatively assigned to the 996-keV transition. The magnetic nature of the 813- and 1067-keV transitions has been confirmed from our polarization measurements [Fig. 3(b)].

As all the prompt transitions above the 11^- isomeric level in Sequence I have been observed for the first time,

the procedure described in Refs. [11,26,27] has also been adopted for multipolarity assignments; this method allows the use of a gating transition with unknown multipolarity. With this procedure, the 1774-keV transition indicates a quadrupole nature ($R_{\rm asym} \sim 0.6$, where $R_{\rm asym} = \frac{I_{\gamma_1} \text{ at } 90^\circ; \text{ gatedwith } \gamma_2 \text{ at } 60^\circ \text{ and } 120^\circ}{I_{\gamma_1} \text{ at } 150^\circ, 210^\circ \text{ and } 325^\circ; \text{ gatedwith } \gamma_2 \text{ at } 60^\circ \text{ and } 120^\circ}$). This transition was then subsequently used as the gating transition in determining the DCO ratio for some of the prompt transitions placed above it.

The angular correlation and polarization measurements for the 607-keV transition indicate that it involves a spin change of $\Delta J = 1$ and is predominantly magnetic in nature. However, this assignment is not unambiguous because of the absence of any prompt coincident transition of known multipolarity. The $\Delta J = 1$ nature of the previously known 584-keV transition is tentative, and the observed statistics did not permit us to assign parity to the level deexcited by this transition. However, shell model calculations, discussed in the subsequent section, predict a (13_2^-) state at this excitation energy. Since the predicted 13_3^- state is in close agreement with the observed 13^- level at E_x = 3654 keV, the level at E_x = 3072 keV is tentatively assigned $J^\pi = (13_2^-)$.

In the present work, the following transitions with energies in keV and multipolarities in parentheses, viz., 282($M1$), 300($M1$), 587($E1$), 598($M1$), 633($M1$), 744($M1$), 933($E2$), 1026($E2$), 1774($E2$), 1903($E2$), and 2744($E2$), have been observed and placed in Sequence I of the ^{90}Nb level scheme. The multipolarity assignment for the 1903-keV transition suggests a spin change of $\Delta J = 2$. However, the present statistics did not permit us to deduce the polarization information for the same. Therefore, the spin assignment of $J^\pi = 15^{(-)}$ to the level deexciting via the 1903-keV transition is tentative. However, this is consistent with the observed parallel decay paths from this level.

The polarization data for the 587-keV transition is indicative of this being an electric transition [Fig. 3(b)]. Hence, the level at $E_x = 6742$ keV is assigned $J^\pi = 17^{(+)}$. The 282- and 744-keV transitions lying above this level, however, are magnetic and have $\Delta J = 1$. The 1026-keV cross-over transition has been assigned an $E2$ multipolarity in conformity with the assignment of $M1$ multipolarity to both the 282- and 744-keV transitions.

In Sequence II, we placed the following transitions with energies (in keV) and multipolarities in parentheses: 163($M1$), 203($E1$), 323($M1$), 990($E1$), 1271($M1$), and 1455($E1$). Earlier workers [7] had assigned an $M1$ multipolarity to the 203-keV transition. The $\Delta J = 1$ nature of this transition has been confirmed from our angular correlation measurements. However, the polarization measurements [Fig. 3(b)] indicate an electric nature for this transition. Hence, we have assigned it an $E1$ electromagnetic nature, and hence, the level at E_x = 855 keV is now assigned a spin and parity of $J^\pi = 2^-$. This level was earlier assigned as $J^\pi = 2^{(+)}$ [28]. From Fig. 3(b), the electric nature of the 1455-keV transition is confirmed, and hence, the level at $E_x = 2309$ keV is assigned a $J^\pi = 3^+$. The parity of the level deexciting via the 990-keV transition is tentatively assigned following the prediction of shell model calculations.

B. Lifetime measurements

The half-life of the $J^\pi = 11^-$ isomeric level in ^{90}Nb was obtained from the analysis of the $E_{d\gamma}$-t matrix. This level deexcites via the 1067-, 71-, 996-, and 813-keV transitions. Fig. 4(a) illustrates the total mass spectrum, as registered in the MWPC; the corresponding γ gated mass spectrum is shown in Fig. 4(b). This information was useful in ascertaining the contamination, if any, from the neighboring nuclei in the observed delayed γ events. The decay curves obtained for the 813- and 1067-keV γ rays following the decay of the $J^\pi = 11^-$ isomeric level in ^{90}Nb are shown in Fig. 5. The estimated half-life of the 11^- isomeric level from the present work is $T_{1/2} = 0.47(1)$ μs, which is in agreement with the value obtained by earlier workers [7,8]. These measurements do not reveal the presence of another isomer in this nucleus as proposed by Fields *et al*. [7].

The $17/2^-$ isomeric level in ^{91}Nb was also populated in the present work. The estimated half-life of the isomeric level is $T_{1/2} = 3.3(4)$ μs, which also agrees with the earlier reported values [8,24].

IV. DISCUSSION AND SHELL MODEL RESULTS

The level structure of ^{90}Nb exhibits characteristics of (multi)particle-hole excitations that are expected to be suitably described by the spherical shell model. Further, the irregular spacing of the observed levels and the presence of high-energy γ rays with $E_\gamma \sim 2$ MeV are indicative of the persistence of the single-particle nature up to the highest observed excitation energy and spin. Thus, the shell model is an appropriate framework to understand the observed level structure.

The $\pi(g_{9/2})\nu(g_{9/2})^{-1}$ and $\pi(p_{1/2})\nu(g_{9/2})^{-1}$ multiplets are expected to dominate the observed low-lying level structure in ^{90}Nb, up to $J \sim 12\hbar$ and $E_x \sim 3$ MeV, as revealed by the calculations of Serduke, Lawson, and Gloeckner [1] and Gross and Frenkel [2].

We have performed shell model calculations using the code OXBASH [29]. The calculations were performed within the π, $\nu(2p_{1/2}, 1g_{9/2})$ valence space outside the ^{76}Sr core. The two-body matrix elements used were code named SLGM in OXBASH. We found a reasonable agreement between the calculated and the observed excitation energies for the low-lying levels (up to $J \sim 13\hbar$) in Sequences I and II, except for the 3^- and (12_2^-) states. The observed high spin states beyond the (13_1^-) level could not be reproduced within this limited model space.

The presence of high-energy ($E_\gamma \sim 2$ MeV) γ rays at low spins clearly indicate the possibility of excitation of protons across the $Z = 38$ subshell closure [10,11], rendering the inclusion of $\pi(1f_{5/2}, 2p_{3/2})$ orbitals quite desirable for a reasonable description of even the low-lying levels (up to $J \sim 10\hbar$).

We have, therefore, performed further calculations using ^{66}Ni as the core and $\pi(1f_{5/2}, 2p_{3/2}, 2p_{1/2}, 1g_{9/2})$ and $\nu(2p_{1/2}, 1g_{9/2}, 1g_{7/2}, 2d_{5/2}, 2d_{3/2}, 3s_{1/2})$ valence orbitals. The two-body matrix elements used were code named GWBXG. Calculations with such a large model space are computationally prohibitive, necessitating some truncation of the

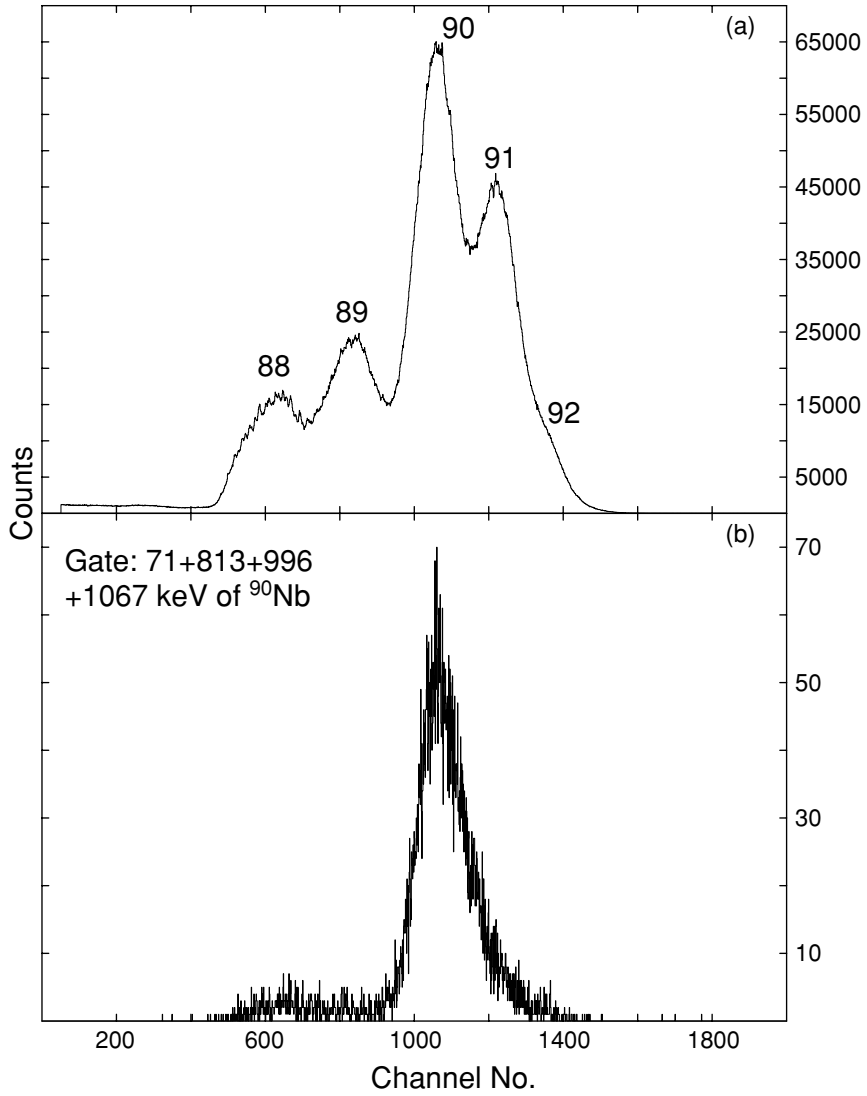

FIG. 4. (a) Mass spectrum as recorded by the MWPC, placed at the focal plane of HIRA when it was tuned for $A = 90$ as the central mass. (b) Corresponding mass spectrum gated by the delayed transitions, belonging to ^{90}Nb.

model space. In our procedure, initially the valence nucleons were allowed to occupy the $\pi(1f_{5/2}, 2p_{3/2}, 2p_{1/2}, 1g_{9/2})$ and $\nu(2p_{1/2}, 1g_{9/2})$ orbitals. However, the predicted excitation energies for the higher spin levels were suppressed when compared with the observed energies. A close inspection revealed that wave functions even for the low-lying levels (including the ground state) were highly fragmented. Further, previous calculations by Gloeckner [30] had clearly pointed to the need to include excitations of neutrons to the $2d_{5/2}$ and $3s_{1/2}$ orbitals, and calculations within the full $\pi(fpg) \otimes \nu(pg)$ model space had indicated that configurations arising from excitation of more than three protons from the $1f_{5/2}$ orbital and more than two protons from the $2p_{3/2}$ orbital do not contribute significantly to the wave functions.

In light of the above, calculations were performed by incorporating all the partitions belonging to $\pi[(1f_{5/2})^{3-6}, (2p_{3/2})^{2-4}, (2p_{1/2})^{0-2}, (1g_{9/2})^{1-8}]$ and $\nu[(2p_{1/2})^{1-2}, (1g_{9/2})^{9-10}]$ configurations[1]; neutron excitation to the $(2d_{5/2}, 3s_{1/2})$ subspace, however, was not allowed. These calculations are referred to as SM1 in the subsequent discussions. Indeed, the SM1 calculation gives almost the same results for the energy eigenvalues as those obtained by calculations with the full $\pi(1f_{5/2}2p_{3/2}2p_{1/2}1g_{9/2})^{13} \otimes \nu(2p_{1/2}1g_{9/2})^{11}$ space, and this similarity between the SM1 and the full $\pi(fpg) \otimes \nu(pg)$ calculations helped us identify the dominant configurations for the observed level structure.

Calculated level energies are compared with the observed levels in Figs. 6 and 7. It is clear from Fig. 6 that the order of the observed negative parity levels is well reproduced in these calculations. Energy eigenvalues of the 9^-, 11^-, (13_2^-), and 13_3^- states are also well reproduced. Except for the 13_3^- level, these states are dominated by the $\pi(1f_{5/2}^6, 2p_{1/2}^4, 2p_{1/2}^1, 1g_{9/2}^2) \otimes \nu(2p_{1/2}^2, 1g_{9/2}^9)$ configurations. Partitions involving excitations of protons from $1f_{5/2}$ and $2p_{3/2}$ orbitals have little influence on these levels. For other levels, the discrepancy varies between 600 and 1600 keV with $E_{\text{theo}}(J^\pi)$ always being under predicted.

Similar observations also hold for the positive parity states. Low-lying positive parity levels (up to $J \sim 9\hbar$) are

[1]The notation $(1f_{5/2})^{n1-n2}$ denotes the minimum $(n1)$ and the maximum $(n2)$ number of particles allowed in the orbital $1f_{5/2}$.

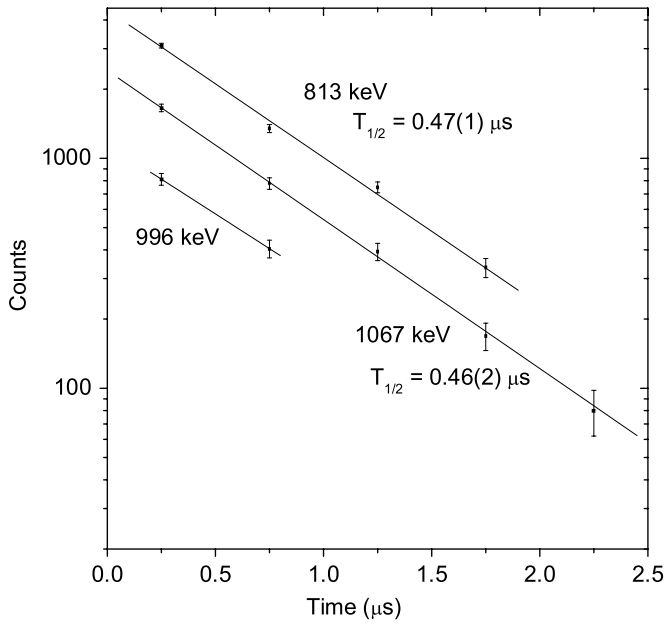

FIG. 5. Decay curves for 813-keV ($9^+ \rightarrow 8^+$) and 1067-keV ($11^- \rightarrow 9^+$) transitions deexciting the 11^- isomeric level in ^{90}Nb. A half-life of 0.47 ± 0.01 μs for the 11^- isomeric level is obtained from this measurement. A similar decay pattern is followed by the 996-keV ($9^- \rightarrow 9^+$) transition. Quoted uncertainties include statistical and fitting errors.

reasonably well reproduced by the calculations. Even though the order of the observed positive parity levels at higher spins is reproduced by the calculations, the predicted excitation energies are compressed in comparison with the observed ones, this discrepancy being maximum for the $15^{(-)}$, $16^{(-)}$, $17^{(+)}$, and $18^{(+)}$ levels.

From the structure of the wave functions, we observe that the ground state and levels up to 9^+, for which a reasonable agreement is observed between the experiment and shell model calculation, have a substantial contribution ($\sim$20–30%) from configurations involving excitation of one or two protons from the $1f_{5/2}$ and $2p_{3/2}$ orbitals. These configurations contribute even more significantly to the wave function of the $3_2^{(+)}$, 3_3^+, and 10^+ to 18^+ states. The $17^{(+)}$, $18^{(+)}$, and $19^{(+)}$ states are constituted solely from these type of partitions coupled to the $\nu(2p_{1/2}^2, 1g_{9/2}^9)$ configuration. Similar observations can also be made for most of the negative parity states.

From the systematics in the neighboring $N = 49$ isotones (viz., ^{92}Tc [31], ^{94}Rh [32]), an yrast 10^+ level is expected at $E_x \sim 1450$ keV. The shell model calculations predict the yrast 10^+ level at $E_x = 1436$ keV. However, the experimentally observed yrast 10^+ level is at 1985 keV.

In order to improve the calculations further, the neutron subspace was slightly extended to include excitations of a single neutron from the $2p_{1/2}, 1g_{9/2}$ orbitals to either $2d_{5/2}$ or $3s_{1/2}$ orbitals (i.e., into the next major oscillator shell). However, calculations involving the $\pi[(1f_{5/2})^{3-6}, (2p_{3/2})^{2-4}, (2p_{1/2})^{0-2}, (1g_{9/2})^{1-8}]$ and $\nu[(2p_{1/2}, 1g_{9/2})^{10} \otimes (2d_{5/2}, 3s_{1/2})^1]$ configurations are computationally prohibitive and require further restriction on the occupancy of the proton particles in the given proton subspace. The dominant proton partitions from the SM1 calculations were identified and coupled with the $\nu(2p_{1/2}, 1g_{9/2})^{11}$ configurations. These calculations are referred to as SM2 (Figs. 6 and 7).

A comparison of the results of SM1 and SM2 with the observed level structure indicates that whereas the negative parity states with $J > 15\hbar$ are well reproduced in SM2, it is SM1 that gives better agreement for the lower spin levels. A plausible explanation could be that inclusion of some

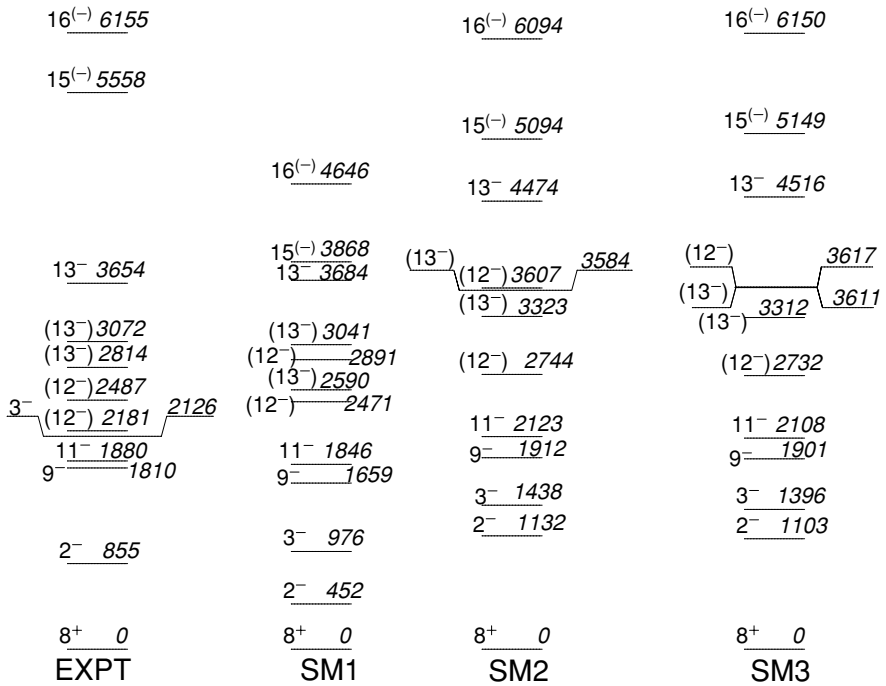

FIG. 6. Comparison of the negative parity levels of ^{90}Nb with the predictions of shell model calculations; refer to text for details.

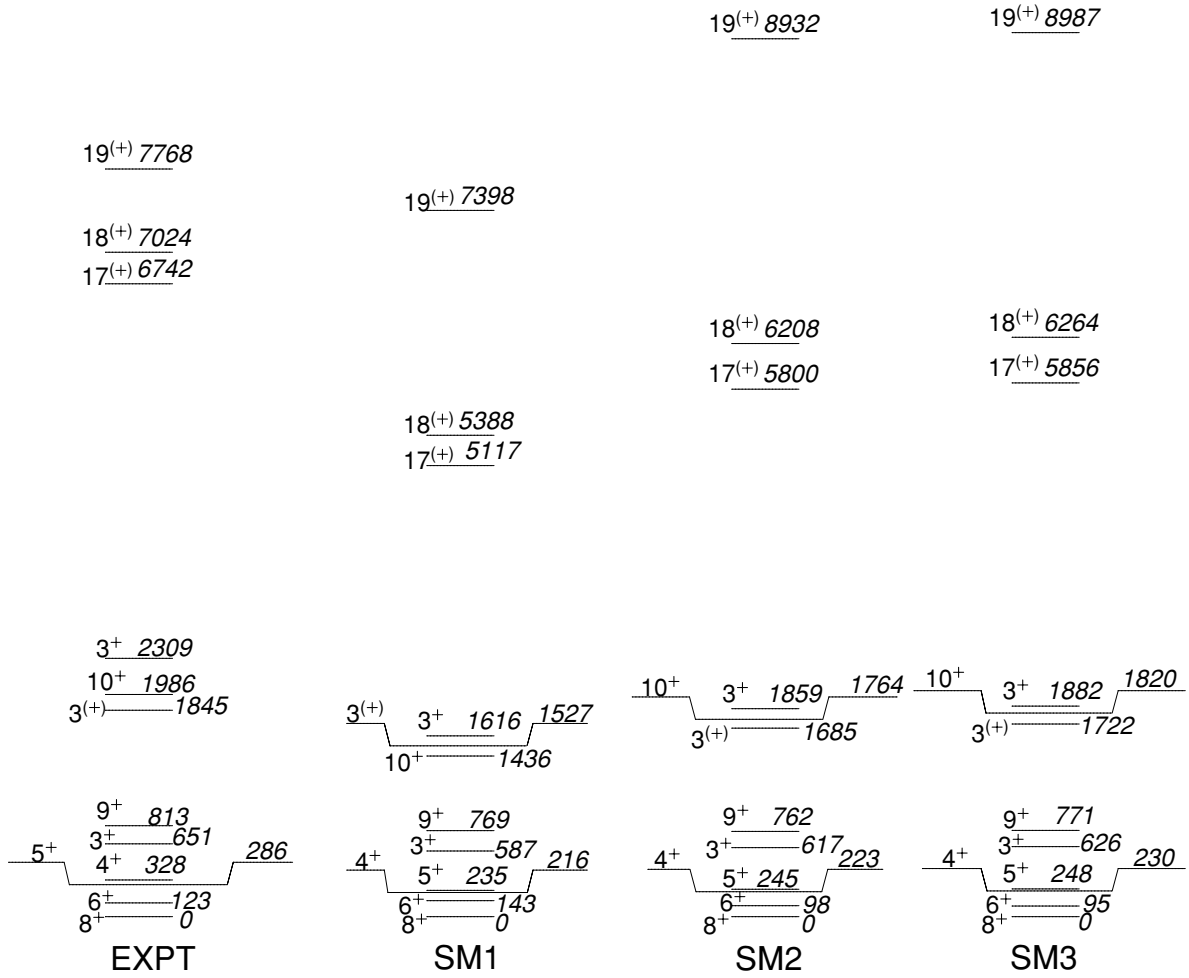

FIG. 7. Same as Fig. 6, but for positive parity levels.

more partitions involving proton excitations from $1f_{5/2}$ and $2p_{3/2}$ orbitals is essential for states with $J < 15\hbar$. Further, for the positive parity levels, SM2 is clearly an improvement over SM1. These comparisons helped to identify the dominant proton configurations, which were then coupled to the $\nu(2p_{1/2}, 1g_{9/2})^{10-11} \otimes (2d_{5/2}, 3s_{1/2})^{0-1}$ configurations. These calculations are referred to as SM3. As seen from Figs. 6 and 7, SM3 indicates only a marginal improvement compared with SM2 in terms of the predicted excitation energies. The wave functions of the observed states have a contribution of less than 1% from the configurations involving a neutron excitation to the $2d_{5/2}$ or $3s_{1/2}$ orbital. However, these configurations are essential to reproducing the observed transition probabilities and branching ratios, as discussed in the subsequent section.

The SM1, SM2, and SM3 calculations indicate that most of the states are dominated by the $\pi(1g_{9/2})\nu(1g_{9/2})^{-1}$ and/or $\pi(2p_{1/2})\nu(1g_{9/2})^{-1}$ $\pi\nu$ multiplets coupled to the states in $^{88}_{38}\mathrm{Sr}_{50}$. However, the higher angular momentum states, e.g., (12_2^-), 13_3^-, $15^{(-)}$, $17^{(+)}$, $18^{(+)}$, and $19^{(+)}$, have a substantial contribution involving proton excitations across the $Z = 38$ subshell closure, i.e., excitations from the $1f_{5/2}$, $2p_{3/2}$ orbitals to $2p_{1/2}$, $1g_{9/2}$ orbitals.

The wave functions obtained in SM1, SM2, and SM3 calculations have been used to estimate the transition probabilities for the decay of the isomeric levels in ^{90,91}Nb. Different sets of effective charges employed in these calculations are summarized in Table II.

In SM1, the substantial reduction in e_p for ^{90}Nb could be attributed to the enlarged proton space. For ^{91}Nb, no similar reduction in e_p is required to reproduce the experimentally observed $B(E2; 17/2^- \rightarrow 13/2^-)$. Indeed, the value of $e_p = 0.77$ (as observed in ^{90}Nb) does not reproduce the experimentally observed transition probability in ^{91}Nb. The observed difference in e_p for the two nuclei is attributed to the presence of the $\nu 1g_{9/2}^{-1}$ configuration in ^{90}Nb. One may conjecture that the presence of this hole may result in a different polarizing effect on the core, as well as on the valence configurations. This is manifested in the lower effective charge for the protons in ^{90}Nb.

Using the set of effective charges reported in Ref. [1], the experimental $B(E2; 11^- \rightarrow 9^-)$ for ^{90}Nb is reproduced well in SM2. This may be attributed to the exclusion of low-lying $1f_{5/2}, 2p_{3/2}$ proton orbitals in the latter calculation. Thus, the present configurations are very similar to those within the $(2p_{1/2}, 1g_{9/2})$ model space, except

TABLE II. Experimental vs theoretical γ-ray transition strengths for isomers in ^{90,91}Nb.

Configuration space	Nucleus	$J_f^\pi \rightarrow J_i^\pi$	$B(E2)_{\text{expt}}$ (e^2 fm^4)	$B(E2)_{\text{theory}}$ (e^2 fm^4)	e_p[a]	e_n[a]
SM1	^{90}Nb	$11^- \rightarrow 9^-$	7.79 ± 0.12	7.85	0.77	0.0
SM2				7.81	1.72	1.67
SM3				7.08–6.76	1.7–1.9	1.0–0.8
SM1	^{91}Nb	$17/2^- \rightarrow 13/2^-$	36.12 ± 4.40	32.96–41.72	1.60–1.80	0.0
SM2				31.28–41.37	2.0–2.3	0.0
SM3				31.40–41.84	1.9–2.2	0.5–0.9

[a]Effective charges e_p and e_n are expressed in units of e.

for a few configurations involving $\pi(1f_{5/2}, 2p_{3/2}) \rightarrow \pi(pg)$ excitations.

As shown in Table II, SM1, SM2, and SM3 calculations successfully reproduce the $B(E2; 17/2^- \rightarrow 13/2^-)$ for ^{91}Nb with the respective set of effective charges. It can also be seen that the SM3 calculation can successfully reproduce the experimental $B(E2)$ values for the isomeric transitions in both ^{90,91}Nb with the same set of effective charges $e_p \sim 1.9$ and $e_n = 0.9$. This is attributed to neutron excitations from the $\nu(2p_{1/2}, 1g_{9/2})$ orbitals to the $2d_{5/2}$ or $3s_{1/2}$ orbital above the $N = 50$ shell closure. The small dependence of $B(E2)$ on the neutron effective charge indicates the relatively lower contribution of configurations involving $\nu(2d_{5/2}, 3s_{1/2})^1$ occupancies.

Obtaining various sets of effective charges for the same $E2$ transition reflects the fact that the effective charges are dependent on the model space used, the occupancy of the orbitals within the model space, and the parametrization of the Hamiltonian. The wave functions and the sets of effective charges derived from the $11^- \rightarrow 9^-$ isomeric transition in ^{90}Nb have been tested further by calculating the branching of the $15^{(-)}$ level (in Sequence I) to the (13_1^-) and 13_3^- levels. The calculated branching in SM3 is $\sim$23% and $\sim$77% for $15^{(-)} \rightarrow (13_1^-)$ and $15^{(-)} \rightarrow 13_3^-$ transitions, respectively. This is in good agreement with the observed branchings, i.e., 32% for $15^{(-)} \rightarrow (13_1^-)$ and 68% for $15^{(-)} \rightarrow 13_3^-$. The calculated branching ratio in SM1 for the same transitions compares poorly with the experimental value, whereas SM2 predicts a value that deviates from the experiment by a factor of 2. It is observed that the experimental branching ratio for the $15^{(-)}$ level is reproduced successfully *only* within the slightly extended neutron model space. This further corroborates the need to include more such configurations to obtain better agreement for the higher spin levels.

V. CONCLUSIONS

The level structure of ^{90}Nb has been extended to $J \sim 19\hbar$ and $E_x \sim 8$ MeV using the conventional prompt $\gamma\gamma$ as well as the prompt-delayed coincidences. Large-basis shell model calculations show that the structure of the higher spin levels can be essentially understood in terms of the proton excitations across the $Z = 38$ subshell closure. However, the structure is also influenced by the configurations arising due to the excitation of neutrons across the $N = 50$ shell closure. The half-lives of the 11^- and $17/2^-$ isomeric levels in ^{90,91}Nb, respectively, have been measured using the recoil-isomer tagging technique. The measured $B(E2)$ for the 11^- isomeric level in ^{90}Nb has been used to extract the effective charges, which were, in turn, used to calculate the branching ratio of the $15^{(-)}$ level to the (13_1^-) and 13_3^- levels, respectively. Only the SM3 calculation, which includes some partitions involving a neutron excitation from the $\nu(pg)$ to the $2d_{5/2}$ or $3s_{1/2}$ orbital, can account for the experimental branching ratio. Inclusion of partitions involving additional proton excitations from the $\pi(1f_{5/2}, 2p_{3/2})$ to $\pi(2p_{1/2}, 1g_{9/2})$ orbitals and neutron excitations from the $\nu(2p_{1/2}, 1g_{9/2})$ to $\nu(1g_{7/2}, 2d_{5/2}, 2d_{3/2}, 3s_{1/2})$ orbitals might be useful for a more complete description of the observed level structure.

ACKNOWLEDGMENTS

The authors would like to thank all the participants in the joint national effort to set up the Clover array at TIFR, Mumbai, and at NSC, New Delhi. The help received from the accelerator staff at TIFR and NSC is gratefully acknowledged. The authors also thank Dr. I. Ray for her help with the ANGCOR code. This work was supported in part by the INDO-US, DST-NSF (Grant No. DST-NSF/RPO-017/98) and by the U.S. National Science Foundation (Grant No. INT-01115336).

[1] F. J. D. Serduke, R. D. Lawson, and D. H. Gloeckner, Nucl. Phys. **A256**, 45 (1976).
[2] R. Gross and A. Frenkel, Nucl. Phys. **A267**, 85 (1976).
[3] S. I. Hayakawa, W. L. Fadner, J. J. Kraushaar, and E. Rost, Nucl. Phys. **A139**, 465 (1969).
[4] J. R. Comfort, H. T. Fortune, G. C. Morrison, and J. V. Maher, Phys. Rev. C **10**, 2399 (1974).
[5] C. A. Fields, R. A. Ristinen, L. E. Samuelson, and P. A. Smith, Nucl. Phys. **A385**, 449 (1982).
[6] Y. Yoshida, M. Ogawa, T. Hattori, H. Taketani, H. Ogata, and I. Kumabe, Nucl. Phys. **A187**, 161 (1972).
[7] C. A. Fields, F. W. N. de Boer, J. J. Kraushaar, R. A. Ristinen, L. E. Samuelson, and E. Sugarbaker, Nucl. Phys. **A363**, 311 (1981).

[8] O. Häusser, T. Faestermann, I. S. Towner, T. K. Alexander, H. R. Andrews, J. R. Beene, D. Horn, D. Ward, and C. Broude, Hyperfine Interact. **4**, 196 (1978).
[9] E. Browne, Nucl. Data Sheets **82**, 379 (1997); **83**, 285(E) (1998).
[10] S. Ray, N. S. Pattabiraman, R. Goswami, S. S. Ghugre, A. K. Sinha, and U. Garg, Phys. Rev. C **69**, 054314 (2004).
[11] N. S. Pattabiraman, S. N. Chintalapudi, S. S. Ghugre, B. V. Tirumala Rao, M. L. N. Raju, T. S. Reddy, P. K. Joshi, R. Palit, and H. C. Jain, Phys. Rev. C **65**, 044324 (2002).
[12] M. Hausmann *et al*., Phys. Rev. C **68**, 024309 (2003).
[13] A. K. Sinha, N. Madhavan, J. J. Das, P. Sugathan, D. O. Kataria, A. P. Patro, and G. K. Mehta, Nucl. Instrum. Methods Phys. Res. A **339**, 543 (1994).
[14] A. Chakraborty *et al*., Phys. Rev. C **70**, 014311 (2004).
[15] S. Nath and N. Madhavan, *Proceedings of DAE-BRNS Symposium on Nuclear Physics* (Varanasi, 2004), edited by P. Singh and L. M. Pant, Vol. 47B, p. 584.
[16] N. S. Pattabiraman, S. N. Chintalapudi, and S. S. Ghugre, Nucl. Instrum. Methods Phys. Res. A **526**, 432 (2004).
[17] N. S. Pattabiraman, S. N. Chintalapudi, and S. S. Ghugre, Nucl. Instrum. Methods Phys. Res. A **526**, 439 (2004).
[18] D. C. Radford, Nucl. Instrum. Methods Phys. Res. A **361**, 297 (1995).
[19] A. Krämer-Flecken, T. Morek, R. M. Lieder, W. Gast, G. Hebbinghaus, H. M. Jäger, and W. Urban, Nucl. Instrum. Methods Phys. Res. A **275**, 333 (1989).
[20] Ch. Droste, K. Starosta, A. Wierzchucka, T. Morek, S. G. Rohoziński, J. Srebrny, M. Bergström, B. Herskind, and E. Wesolowski, Nucl. Instrum. Methods Phys. Res. A **430**, 260 (1999).
[21] K. Starosta *et al*., Nucl. Instrum. Methods Phys. Res. A **423**, 16 (1999).
[22] M. K. Kabadiyski *et al*., Z. Phys. A **343**, 165 (1992).
[23] T. Rzaca-Urban *et al*., Nucl. Phys. **A579**, 319 (1994).
[24] B. A. Brown, P. M. S. Lesser, and D. B. Fossan, Phys. Rev. C **13**, 1900 (1976).
[25] H. Morinaga and T. Yamazaki, *In-Beam Gamma-Ray Spectroscopy* (North-Holland, Amsterdam, 1976).
[26] P. Singh, R. G. Pillay, J. A. Sheikh, and H. G. Devare, Phys. Rev. C **45**, 2161 (1992).
[27] H. Harada, M. Sugawara, H. Kusakari, H. Shinohara, Y. Ono, K. Furuno, T. Hosoda, M. Adachi, S. Matsuki, and N. Kawamura, Phys. Rev. C **39**, 132 (1989).
[28] R. B. Firestone *et al*., *Table of Isotopes*, Eighth Ed. (Wiley, New York, 1996).
[29] B. A. Brown, A. Etchegoyen, W. D. M. Rae, and N. S. Godwin, computer code OXBASH, 1984.
[30] D. H. Gloeckner, Nucl. Phys. **A253**, 301 (1975).
[31] A. A. Tulapurkar, P. Das, S. N. Mishra, R. G. Pillay, and J. A. Sheikh, Phys. Rev. C **54**, 2904 (1996).
[32] S. E. Arnell, D. Foltescu, H. A. Roth, Ö. Skeppstedt, J. Blomqvist, A. Nilsson, T. Kuroyanagi, S. Mitarai, and J. Nyberg, Phys. Rev. C **49**, 51 (1994).